AIAA JOURNAL
Vol. 31, No. 10, October 1993

Three-Dimensional Navier-Stokes/Full-Potential Coupled Analysis for Viscous Transonic Flow

Lakshmi N. Sankar*
Georgia Institute of Technology, Atlanta, Georgia 30332
Bala K. Bharadvaj†
Douglas Aircraft Company, Long Beach, California 90846
and
Fu-Lin Tsung‡
Georgia Institute of Technology, Atlanta, Georgia 30332

A novel technique for the prediction of three-dimensional steady and unsteady viscous flows past arbitrary configurations is described. The flowfield is partitioned into an inner region adjacent to the solid surface and an outer region away from the solid surface. The solution procedure uses a three-dimensional compressible Navier-Stokes solver in the inner vortical region and a three-dimensional unsteady full-potential flow solver in the outer irrotational region. These two solvers are tightly coupled and integrated simultaneously in time. This coupled analysis enables efficient and accurate computation of transonic flows, including unsteady viscous effects. In the present work, details of the coupling procedure are described, along with numerical validation of the coupled formulation. Computational results are presented for an airplane wing as well as for a helicopter rotor in hover; these are compared with experimental data and other computational fluid dynamics data. The present coupled analysis requires only about 50% of the CPU time needed by a standard Navier-Stokes analysis and generates equally accurate data.

Nomenclature

A, B	= Jacobian matrices
a	= speed of sound
b	= half-span
$\hat{E}$, $\hat{F}$, $\hat{G}$	= inviscid flux vectors
$\hat{E}v$, $\hat{F}v$, $\hat{G}v$	= viscous flux vectors
I	= identity matrix
i, j, k	= grid indices in chordwise, spanwise, and normal directions, respectively
J	= Jacobian of transformation from Cartesian to curvilinear system
L, U	= lower and upper matrices
M	= Mach number
$\hat{Q}$	= vector of conserved variables for the Navier-Stokes equations
R	= rotor blade radius
$\boldsymbol{R}$	= residual matrix
r	= radial station on rotor blade
t	= time, in inertial frame
U, V, W	= contravariant velocities in ξ, η, ζ directions, respectively
x, y, z	= Cartesian coordinates
α	= angle of attack
$\Delta(\ldots)$	= finite jump in ...
ξ, η, ζ	= curvilinear coordinate system
ρ	= density
τ	= time, in moving frame
φ	= inviscid disturbance velocity potential

Subscript and Superscript

∞	= freestream value
n	= integration time level

Presented as Paper 91-1595 at the AIAA 10th Computational Fluid Dynamics Conference, Honolulu, HI, June 24-27, 1991; received Sept. 29, 1992; revision received March 16, 1993; accepted for publication March 20, 1993.

*Professor, School of Aerospace Engineering. Senior Member AIAA.

†Senior Principal Engineer Scientist, Aircraft Structure. Associate Fellow AIAA.

‡Graduate Research Assistant, School of Aerospace Engineering. Student Member AIAA.

Introduction

COMPUTATIONAL methods for the prediction of unsteady transonic flow past isolated wings and wing-body configurations have matured rapidly during the past decade. A variety of mathematical models and computer codes are currently available based on transonic small disturbance (TSD),[1,2] transonic full-potential analysis,[3-5] Euler equations,[6,7] and Navier-Stokes equations.[8,9] Among these various formulations, the TSD-based methods have made the most progress in modeling complex configurations, and the full-potential methods with interactive boundary layers[10-12] have proven useful for analyzing thick wings and wing-body configurations at reasonable computational cost. Methods based on solution of the complete Navier-Stokes equations are currently used primarily to study physical phenomena, such as high angle-of-attack aerodynamics of highly swept wings, since they are too expensive for routine prediction of steady and unsteady airloads.

Although the full-potential method with interactive boundary layer is quite useful for analysis at low angles of attack, this approach becomes inadequate for many practical situations. Examples of flows where the full-potential analysis with interactive boundary layer is not adequate include shock-induced boundary-layer separation and extensive separations that occur over control surfaces at large deflection and downstream of a spoiler mounted on the wing surface. For unsteady flows involving significant shock motion, the use of boundary-layer theory based on steady flow assumptions may become questionable. Hence, there is a need for developing solution techniques that can predict these types of flows without the significant CPU time and memory requirements associated with a standard Navier-Stokes formulation.

The present work describes a hybrid procedure that can be used to compute flows with significant shock/boundary-layer interaction or large-scale separation by accounting for viscous effects more accurately than the interactive boundary-layer

approach. It makes use of two computer codes previously developed by the present investigators[9,12] to study three-dimensional viscous and inviscid unsteady transonic flows. In this procedure, the flowfield surrounding the wing is divided into two regions. The inner zone consists of the vortical flow region near the body surface and includes areas of strong viscous effects, shock/boundary-layer interaction, and the downstream wake. Located away from the shock waves and the viscous layer, the outer zone, which surrounds the inner region and extends to the far-field boundary, is assumed to be irrotational. The three-dimensional unsteady Navier-Stokes equations are solved in the inner zone using a semi-implicit time-marching algorithm, and the three-dimensional unsteady full-potential equation is solved in the outer region. The flowfields in the two regions are tightly coupled to each other at every time step through the exchange of mass and momentum at the zonal interface.

Formulations

Since the methodologies of the Navier-Stokes analysis and the full-potential approach employed in the present study have been previously documented, only brief outlines of the mathematical formulations are given here.

Navier-Stokes Formulation

The unsteady, compressible Reynolds-averaged Navier-Stokes equations for an inertial Cartesian coordinate system in conservation form can be written as a single vector equation

$$\frac{\partial \hat{Q}}{\partial t} + \frac{\partial(\hat{E} - \hat{E}v)}{\partial x} + \frac{\partial(\hat{F} - \hat{F}v)}{\partial y} + \frac{\partial(\hat{G} - \hat{G}v)}{\partial z} = 0 \tag{1}$$

where $\hat{Q}$ is a vector containing the unknown flow properties such as density, momentum, and energy. The quantities $\hat{E}$, $\hat{F}$, and $\hat{G}$ contain information related to the convective transport of mass, momentum, energy, and the pressure forces. The terms $\hat{E}v$, $\hat{F}v$, and $\hat{G}v$ contain viscous (laminar and turbulent) stress contributions to mass, momentum, and energy transport.

To facilitate the computation of flow past arbitrary configurations such as wings and wing-body combinations, and to account for the motion of these surfaces, Eq. (1) is transformed to a new coordinate system (τ, ξ, η, ζ), in which the solid surfaces such as the wing or fuselage are mapped onto coordinate surfaces. In the transformed coordinate system, the governing equations may be written as

$$\frac{\partial \boldsymbol{Q}}{\partial \tau} + \frac{\partial(\boldsymbol{E} - \boldsymbol{E}v)}{\partial \xi} + \frac{\partial(\boldsymbol{F} - \boldsymbol{F}v)}{\partial \eta} + \frac{\partial(\boldsymbol{G} - \boldsymbol{G}v)}{\partial \zeta} = 0 \tag{2}$$

The quantities $\boldsymbol{Q}$, $\boldsymbol{E}$, $\boldsymbol{F}$, $\boldsymbol{G}$, etc., are derived from their Cartesian counterparts $\hat{\boldsymbol{Q}}$, $\hat{\boldsymbol{E}}$, $\hat{\boldsymbol{F}}$, $\hat{\boldsymbol{G}}$, etc., through the metrics of the transformation and are listed in Ref. 13.

The Navier-Stokes equations are solved by numerical integration, starting from an initial guess for the flow vector $\boldsymbol{Q}$, then marching in time. A finite difference procedure has been used to approximate the various derivatives appearing in Eq. (2). Although second-order accuracy in time and fourth-order accuracy in space are possible with the present formulation, the results presented here are based on a first-order temporal and second-order spatial formulation. The finite difference analog of Eq. (2) at time level n is

$$\Delta \boldsymbol{Q}^{n+1}/\Delta\tau + \delta_\xi \boldsymbol{E}^{n+1} + \delta_\eta \boldsymbol{F}^* + \delta_\zeta \boldsymbol{G}^{n+1} = (\delta_\xi \boldsymbol{E}v + \delta_\eta \boldsymbol{F}v + \delta_\zeta \boldsymbol{G}v)^n \tag{3}$$

where, δ_ξ, δ_η, and δ_ζ are standard symmetric central-difference operators. The quantity $\Delta \boldsymbol{Q}^{n+1}$ is the change in $\boldsymbol{Q}$ during successive time levels. The viscous terms on the right-hand side of the equation are evaluated explicitly at the old time level n. The spanwise derivative $\delta_\eta \boldsymbol{F}^*$ is evaluated semi-explicitly, using values at time level n or time level $(n + 1)$ as soon as they become available.

Equation (3) is a set of nonlinear algebraic equations for the change in flow property $\Delta \boldsymbol{Q}$. To solve for $\Delta \boldsymbol{Q}$, the nonlinear vectors $\boldsymbol{E}$ and $\boldsymbol{G}$ at time level $(n + 1)$ are linearized at every time level about their values at the previous time level n as follows:

$$\boldsymbol{E}^{n+1} = \boldsymbol{E}^n + \boldsymbol{A}^n \Delta \boldsymbol{Q}^{n+1} + \mathcal{O}(\Delta\tau^2) \tag{4a}$$

$$\boldsymbol{G}^{n+1} = \boldsymbol{G}^n + \boldsymbol{B}^n \Delta \boldsymbol{Q}^{n+1} + \mathcal{O}(\Delta\tau^2) \tag{4b}$$

where $\boldsymbol{A}$ and $\boldsymbol{B}$ are 5×5 matrices evaluated at time level n and are given by $\partial \boldsymbol{E}/\partial \boldsymbol{Q}$ and $\partial \boldsymbol{G}/\partial \boldsymbol{Q}$, respectively.

The linearized system of algebraic equations may be written as a system of equations involving the unknown $\Delta \boldsymbol{Q}$ in the following operator form:

$$[\boldsymbol{I} + \Delta\tau(\delta_\xi \boldsymbol{A}^n + \delta_\zeta \boldsymbol{B}^n)]\Delta \boldsymbol{Q}^{n+1} = \boldsymbol{R}^{n,n+1} \tag{5}$$

where the right-hand side is the residual, which contains known information about $\boldsymbol{E}$, $\boldsymbol{F}$, $\boldsymbol{G}$, $\boldsymbol{E}v$, $\boldsymbol{F}v$, and $\boldsymbol{G}v$ from time level n and time level $(n + 1)$ where available. For steady flow applications, an iterative solution to the three-dimensional Navier-Stokes equations requires that the quantity $\boldsymbol{R}$ be driven to zero. For unsteady problems, $\boldsymbol{R}$ is on the order of the time step $\Delta\tau$ and is generally nonzero.

Equation (5) couples the quantity $\Delta \boldsymbol{Q}$ at every point in the flowfield with its four neighboring nodes in the ξ-ζ plane and consists of a large banded matrix with five nonzero block diagonals. Direct inversion of this large bandwidth system is costly; therefore, an alternating direction approximate factorization scheme is used here. This requires factorizing the matrix operator on the left side of Eq. (5) into two smaller operators, leading to the following equation:

$$(\boldsymbol{I} + \Delta\tau\delta_\xi \boldsymbol{A}^n)(\boldsymbol{I} + \Delta\tau\delta_\zeta \boldsymbol{B}^n)\Delta \boldsymbol{Q}^{n+1} = \boldsymbol{R}^{n,n+1} \tag{6}$$

Solving the two block-tridiagonal matrices in Eq. (6) at every time level is significantly less costly than solving the original large bandwidth system of Eq. (5). The solution of the block tridiagonal matrices is obtained efficiently using the well-known Thomas algorithm, which is easily vectorized.

In high Reynolds number flows, the use of standard central differences can cause spatial oscillations to appear at every time step. These high-frequency oscillations can grow if unchecked and can lead to catastrophic failure of the solution. To avoid this, the solution is smoothed at every time step using a weighted formula linking each node to its four neighbors for enhanced stability. In turbulent flows, the laminar viscosity coefficient is augmented with an eddy viscosity coefficient using the Baldwin-Lomax algebraic model. Details on the implementation of these smoothing operations and implementation of the turbulence model are given in Refs. 13 and 14.

Full-Potential Formulation

The three-dimensional unsteady compressible potential flow equation may be written in a curvilinear coordinate system as

$$\left(\frac{\rho}{J}\right)_\tau + \left(\frac{\rho U}{J}\right)_\xi + \left(\frac{\rho V}{J}\right)_\eta + \left(\frac{\rho W}{J}\right)_\zeta = 0 \tag{7}$$

It is possible to express the time derivative of the density term in Eq. (7) as terms with mixed time-space derivatives of the disturbance velocity potential. The resulting equation is

$$\left(\frac{\rho}{a^2 J}\right)(\varphi_{\tau\tau} + U\varphi_{\xi\tau} + V\varphi_{\eta\tau} + W\varphi_{\zeta\tau}) = \left(\frac{\rho U}{J}\right)_\xi + \left(\frac{\rho V}{J}\right)_\eta + \left(\frac{\rho W}{J}\right)_\zeta \tag{8}$$

This equation is hyperbolic in time, and it may be discretized using one-point or two-point backward differences in time.

The spatial derivatives are all approximated using central differences. In supersonic regions, central-difference approximations to spatial derivatives do not correctly represent the physical domain of dependence. To avoid this, the artificial compressibility concept is used, and the density appearing in the term $(\rho U/J)$ is approximated by a weighted combination of the density at a node (i, j, k) and its upstream neighbor $(i-1, j, k)$. This treatment reduces the formal spatial accuracy of the full-potential formulation to first order in supersonic regions.

The discretized form of the previous equation is a 27-point nonlinear equation linking the change in the disturbance potential φ at a node (i, j, k) to its 26 neighbors, such as $(i-1, j, k)$, $(i+1, j, k)$, etc. The nonlinearity is made linear by setting ρ, U, V, and W to be at the old time level and leaving explicit derivatives of φ at the new time level. When the grids are nearly orthogonal, the cross coupling between the node (i, j, k) and the corner nodes such as $(i-1, j+1, k)$ may be ignored, leading to a seven diagonal linearized system of equations for the unknown φ.

In the present work, the seven diagonal system is recast into an equivalent system of LU form using a strongly implicit procedure. The resulting L and U matrices are sparse, which leads to an efficient solution for the system of equations. Additional details on the solution procedure are given in Ref. 3.

Navier-Stokes/Full-Potential Coupling

Figure 1 shows how the flowfield surrounding the isolated wing is partitioned into the inner and outer zones over one-half of the wing. The Navier-Stokes equations are solved in the inner zone, and the full-potential equation is applied to the outer region. The method of partitioning the flowfield is not limited to that shown in Fig. 1. In cases where partially separated flow occurs over deflected control surfaces, it is possible to divide the flowfield into spanwise partitions where the Navier-Stokes formulation is used over the control surfaces

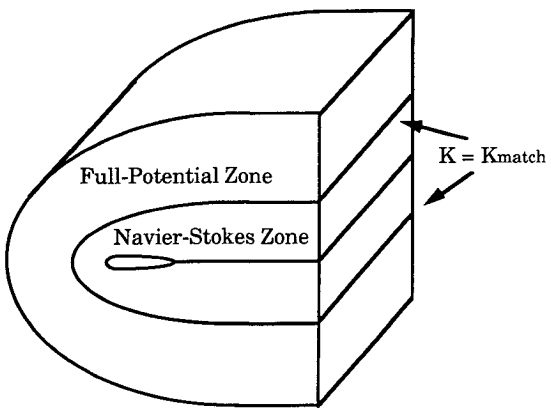

Fig. 1 Schematic diagram of the Navier-Stokes/full-potential domain used in the calculations.

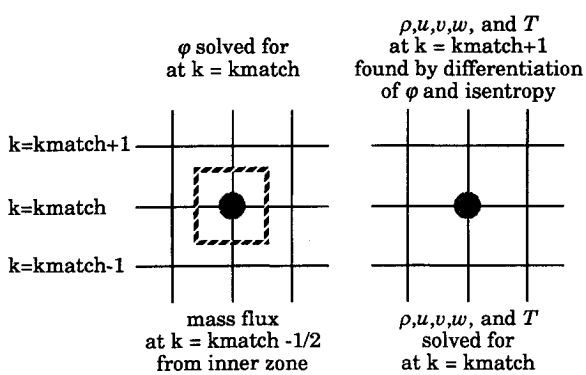

Fig. 2 Computational stencil at the Navier-Stokes and full-potential zonal interface.

and the full-potential analysis (possibly with an interactive boundary layer) is employed everywhere else. In the general case, regions of Navier-Stokes analysis can be imbedded within an overall flowfield that is modeled using the full-potential approach. In the present work, results are presented only for the partitioning illustrated in Fig. 1.

At every time step, physically correct boundary conditions for the flow properties are imposed. On the solid surface, the viscous fluid and the solid have the same velocity; also, the pressure and density gradients vanish at the solid surface. At the far-field boundaries, the flow properties are assumed to return to their freestream conditions.

At every step, information is exchanged between the inner Navier-Stokes region and the outer potential flow region. The plane $k = k_{\text{match}}$ marks the interface between the inner zone and the outer zone. In the present formulation, the Navier-Stokes equations are solved at all nodes up to and including nodes on the plane $k = k_{\text{match}}$. The full-potential equation is solved between the plane $(k_{\text{match}} - 1)$ and the outermost k plane. Thus, the inner and outer regions overlap each other by one plane of cells. Since the two regions overlap rather than abut against each other, boundary conditions for both regions can be specified at the interface without resorting to nonphysical extrapolation of information.

For instance, the Navier-Stokes solver requires the flow properties (the three components of velocity, density, and temperature) at the plane $k = (k_{\text{match}} + 1)$ to solve for the flowfield at the plane $k = k_{\text{match}}$. This information is obtained from the outer (full-potential) solver by the following equations:

$$\begin{aligned} T &= T_\infty(\rho/\rho_\infty)^{\gamma-1} \\ u &= u_\infty + \varphi_\xi \xi_x + \varphi_\eta \eta_x + \varphi_\zeta \zeta_x \\ v &= v_\infty + \varphi_\xi \xi_y + \varphi_\eta \eta_y + \varphi_\zeta \zeta_y \\ w &= w_\infty + \varphi_\xi \xi_z + \varphi_\eta \eta_z + \varphi_\zeta \zeta_z \end{aligned} \tag{9}$$

The terms φ_ξ, φ_η, etc., are found using two-point centered differences rather than one-sided extrapolations, since the velocity potential values are available up to and including the planed $k = (k_{\text{match}} - 1)$.

Similarly, the outer region requires the mass flux and density at a plane $k = (k_{\text{match}} - \frac{1}{2})$ to evaluate the velocity potential at the plane $k = k_{\text{match}}$. This is computed from the inner region using simple averages such as

$$\rho_{k_{\text{match}}-\frac{1}{2}} = (\rho_{k_{\text{match}}-1} + \rho_{k_{\text{match}}})/2 \tag{10}$$

Again, since the inner zone solution includes the plane $k = k_{\text{match}}$, no extrapolation of the inner flowfield is necessary. Figure 2 illustrates the computation stencil for the two regions at the interface.

Other ways of linking the two regions have also been tested. For instance, a Dirichlet-type boundary condition may be prescribed for the outer zone at the plane $k = (k_{\text{match}} - 1)$ by integrating the velocity field computed by the inner solver at the $(k_{\text{match}} - 1)$ plane. Alternatively, the boundary conditions based on the one-dimensional unsteady method of characteristics may be prescribed for either the inner or the outer region.

It may be noted that in unsteady flows the plane $k = k_{\text{match}}$ should be free to float up or down to maximize the potential benefit of the coupled analysis. For example, when a helicopter rotor is in forward flight, the value of k_{match} will be larger on the retreating blade due to the fact that the viscous region is larger and the flow usually involves massive separation. On the advancing side, the value of k_{match} may be dynamically reduced. A similar situation exists in the case of an oscillating control surface; the flow tends to separate when the control surface deflection is large but is well behaved for small deflections. The present algorithm is being extended to provide dynamic reconfiguration of the flowfields into potential and viscous regions without manual intervention by the user.

To maintain the benefits of vectorization, it is preferable to perform the dynamic reconfiguration of the flowfield at the block level rather than at the level of individual nodes. In other words, for each spanwise station, the value of k_{match} is the same for all chordwise stations. This setup allows the code to be vectorized for an entire "i" line at a time.

Results and Discussion

The Navier-Stokes solver and the full-potential solver have both been tested extensively as stand-alone analysis tools for steady and unsteady transonic flow applications. These formulations and results of applications have been documented

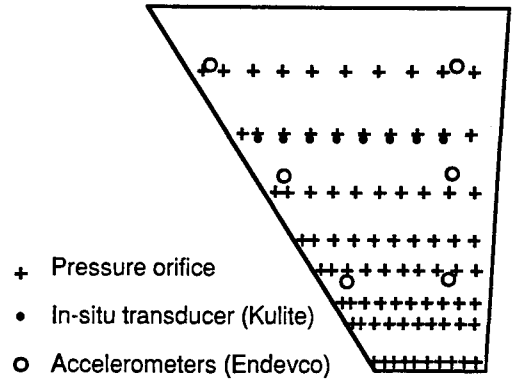

Fig. 3 Planform of the F5 wing, indicating pressure transducer locations.

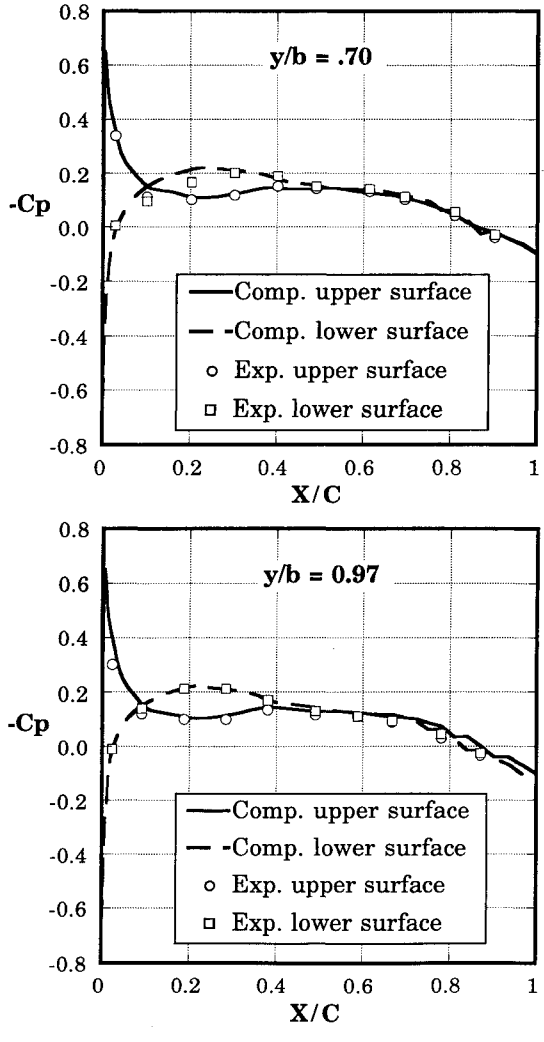

Fig. 4 Comparison of the Navier-Stokes/full-potential equations results with experiment, 0.8 Mach number, zero angle of attack.

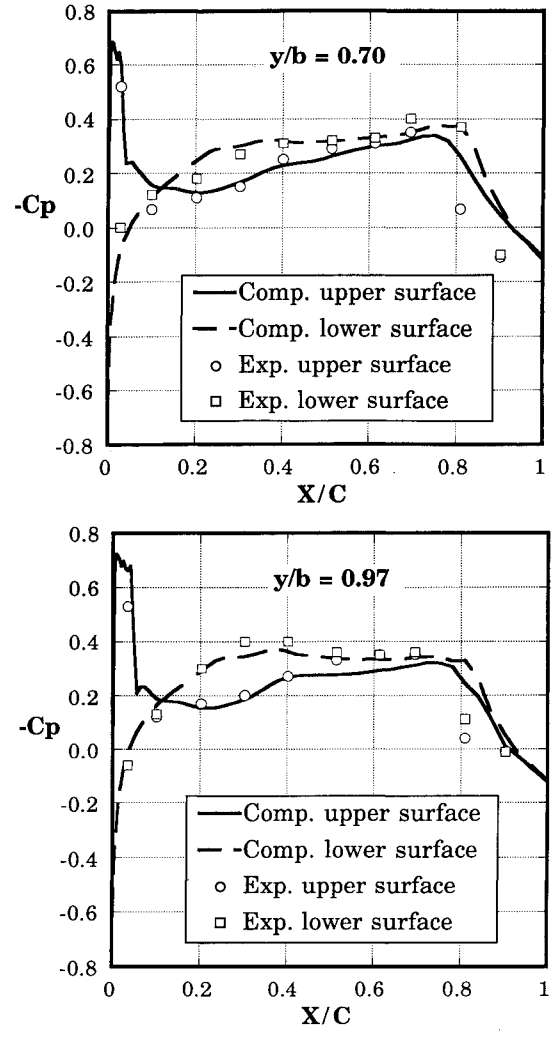

Fig. 5 Comparison of the Navier-Stokes/full-potential equations results with experiment, 0.95 Mach number, zero angle of attack.

in the open literature.[3,9,12] To demonstrate the capability of the coupled algorithm, steady numerical results have been obtained for the F5 wing, as well as for an isolated helicopter rotor in hover. These results are discussed next and compared with experimental data or data from other computational fluid dynamics (CFD) analyses.

The F5 wing planform is shown in Fig. 3. This wing has an aspect ratio of 3.16, leading-edge sweep of 32 deg, and wing sections with a thickness ratio of 4.8%. Extensive steady and unsteady test data are available for this wing.[15] The computational analysis was carried out on a global grid of $121 \times 19 \times 41$ points, of which $81 \times 14 \times 1$ points were used to define the planform geometry. The first point off the planform surface in the normal direction is 0.0001, nondimensionalized by the local chord length. The inner $121 \times 19 \times 21$ part of the grid was used for the Navier-Stokes zone, whereas the outer $121 \times 19 \times 22$ points were used for the full-potential analysis. The airflow was started from rest, and the computations were advanced in a time-accurate manner.

Figure 4 shows the chordwise pressure distributions obtained from the present method for a subcritical flow condition ($M_\infty = 0.80$, $\alpha = 0$ deg) at two span locations. It is shown that the present results are in good agreement with experimental data. As it turns out, even the full-potential approach yields good results for this case since the viscous effects are quite small. However, the current results demonstrate that the coupling procedure is stable and convergent.

Figure 5 shows results for the F5 wing at a freestream Mach number of 0.95. In this case the flow becomes truly transonic,

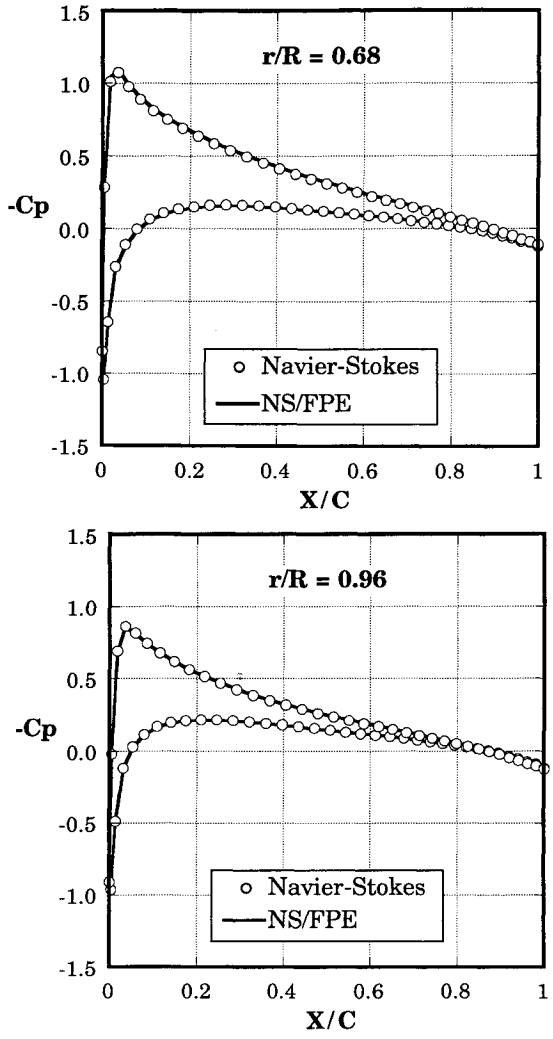

Fig. 6 Comparison of the Navier-Stokes/full-potential equations results with Navier-Stokes solutions for a two-bladed helicopter rotor in hover, 8 deg collective pitch, 0.44 tip Mach number.

and the experimental data show the presence of a shock located at about 80% chord along the entire span. The chordwise pressure distribution computed by the present analysis matches the experimental data over most of the wing, including the location of the shock. The current analysis indicates that the flow separates downstream of the shock. From the experimental data (which are sparse near the trailing edge), it is difficult to conclude if the flow downstream of the shock is attached or separated. Additional studies are needed to clarify this issue.

The coupled procedure was also applied to the case of an isolated two-bladed helicopter rotor in hover. The rotor modeled has a rectangular planform, a blade aspect ratio of 6, and NACA 0012 airfoil sections. Computations were done for the case with a tip Mach number of 0.44, at a collective pitch of 8 deg, using the same number of grids as for the F5 wing. The pressure computed from the present method is shown in Fig. 6 along with data obtained from a standard Navier-Stokes analysis. It may be seen that the two solutions are very similar; however, the present hybrid analysis required only about 50% of the computational time taken by the standard Navier-Stokes procedure, demonstrating the computational efficiency of the hybrid formulation. To illustrate the effectiveness of the interface conditions, the density contour lines across the zonal boundary at a spanwise station are plotted and shown in Fig. 7. The figure shows that at the interface the density varies fairly smoothly across the two regions. Similar smoothness is also observed for other flow variables such as pressure and velocities.

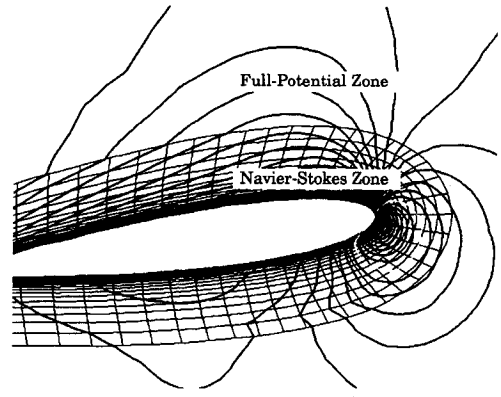

Fig. 7 Density contour across the Navier-Stokes and the full-potential boundary for the rotor at $r/R = 0.76$.

Conclusion

A hybrid computational technique using a coupling of Navier-Stokes and full-potential formulations has been developed. The time-accurate numerical algorithm has been validated by application to the F5 wing for subsonic and transonic conditions and comparison with experimental data. The algorithm has also been applied to the case of a helicopter rotor in hover. The present computational procedure yields results comparable in accuracy to the standard Navier-Stokes analysis at savings of about 50% in the computational effort.

The results presented here constitute only the initial validation of the hybrid procedure and are seen as the stepping stone for further improvements and other steady and unsteady applications involving flow conditions with stronger viscous effects. Future improvements such as dynamic zonal configuration are planned to increase the computational efficiency without decreasing the accuracy of the results.

Acknowledgments

The development of the standard Navier-Stokes code used in this paper was funded by the United States Army Research Office (Tom Doligalski, technical monitor). The full-potential code and the coupling procedure were funded by McDonnell Douglas Corporation under its independent research and development program. The computation resource for the rotor portion was provided by Cray Research.

References

[1]Batina, J. T., "Unsteady Transonic Flow Calculations for Realistic Aircraft Configurations," AIAA/ASME/ASCE/AHS/ASC 28th Structures, Structural Dynamics, and Materials Conference, AIAA Paper 87-0850, Monterey, CA, April 1987.

[2]Guruswamy, G. P., Goorijian, P. M., and Tu, E. L., "Unsteady Transonics of a Wing with Tip Store," *Journal of Aircraft,* Vol. 23, No. 8, 1986, pp. 662-668.

[3]Sankar, L. N., Malone, J. B., and Tassa, Y., "An Implicit Conservative Algorithm for Steady and Unsteady Three-Dimensional Transonic Potential Flows," AIAA Paper 81-1016, June 1981.

[4]Shankar, V., and Ide, H., "Treatment of Steady and Unsteady Flows Using a Fast, Time Accurate Full Potential Scheme," AIAA Paper 85-4060, Oct. 1985.

[5]Malone, J. B., Sankar, L. N., and Sotomayer, W. A., "Unsteady Aerodynamic Modeling of a Fighter Wing in Transonic Flow," *Journal of Aircraft,* Vol. 23, No. 8, 1986, pp. 611-620.

[6]Sankar, L. N., Malone, J. B., and Schuster, D., "Euler Solutions for Transonic Flow past a Fighter Wing," *Journal of Aircraft,* Vol. 24, No. 1, 1987, pp. 10-16.

[7]Batina, J. T., "Development of Unstructured Grid Methods for Steady and Unsteady Aerodynamic Analysis," Inst. for Computer Applications in Science and Engineering, ICASE Paper 90-6.9.4, NASA Langley Research Center, Hampton, VA, Sept. 1990.

[8]Wake, B. E., and Sankar, L. N., "Solution of Navier-Stokes Equations for the Flow About a Rotor Blade," *Journal of the American Helicopter Society,* Vol. 34, No. 2, 1989, pp. 13-23.

[9]Sankar, L. N., and Kwon, O. J., "High-Alpha Simulation of

Fighter Aircraft," *Proceedings of the NASA High-Angle-of Attack Technology Conference, Vol. 1, Pt. 2,* NASA Langley Research Center, Hampton, VA, Oct. 1990, pp. 689–702.

[10]Woodson, S. H., DeJarnette, F. R., and Campbell, J. F., "An Interactive Three-Dimensional Boundary-Layer Method for Transonic Flow over Swept Wings," AIAA Paper 89-0112, Jan. 1989.

[11]Cebeci, T., Chen, L. T., and Chang, K. C., "An Interactive Scheme for Three-Dimensional Transonic Flows," *Numerical and Physical Aspects of Aerodynamic Flows III,* Springer-Verlag, New York, 1986, pp. 412–431.

[12]Bharadvaj, B. K., "Computation of Unsteady Control Surface Loads in Transonic Flow," AIAA Paper 90-0935, April 1990.

[13]Wake, B. E., "Solution Procedure for the Navier-Stokes Equations Applied to Rotors," Ph.D. Dissertation, Georgia Inst. of Technology, Atlanta, GA, April 1987.

[14]Tsung, F.-L., and Sankar, L. N., "Numerical Simulation of Flow Separation for Rotors and Fixed Wings," AIAA Paper 92-0635, Jan. 1992.

[15]Tijdeman, J., et al., "Transonic Wind Tunnel Tests on an Oscillating Wing with External Stores, Part II—Clean Wing," Air Force Flight Dynamics Lab., AFFDL-TR-78-194, Wright-Patterson AFB, OH, March 1979.